Autonomous TNF is critical for in vivo monocyte survival in steady state and inflammation

Yochai Wolf,[1] Anat Shemer,[1] Michal Polonsky,[1] Mor Gross,[1] Alexander Mildner,[1] Simon Yona,[1] Eyal David,[1] Ki-Wook Kim,[1] Tobias Goldmann,[2] Ido Amit,[1] Mathias Heikenwalder,[4,5] Sergei Nedospasov,[6,7] Marco Prinz,[2,3] Nir Friedman,[1] and Steffen Jung[1]

[1]Department of Immunology, Weizmann Institute of Science, Rehovot 76100, Israel
[2]Institute for Neuropathology and [3]BIOSS Centre for Biological Signaling Studies, University of Freiburg, 79085 Freiburg, Germany
[4]Institut für Virologie, Helmholtz Zentrum München, 85764 Neuherberg, Germany
[5]Department of Chronic Inflammation and Cancer, German Cancer Research Center, 69120 Heidelberg, Germany
[6]Engelhardt Institute of Molecular Biology, Moscow, Russia 119991
[7]German Rheumatism Research Center, 10117 Berlin, Germany

Monocytes are circulating mononuclear phagocytes, poised to extravasate to sites of inflammation and differentiate into monocyte-derived macrophages and dendritic cells. Tumor necrosis factor (*TNF*) and its receptors are up-regulated during monopoiesis and expressed by circulating monocytes, as well as effector monocytes infiltrating certain sites of inflammation, such as the spinal cord, during experimental autoimmune encephalomyelitis (EAE). In this study, using competitive in vitro and in vivo assays, we show that monocytes deficient for *TNF* or *TNF* receptors are outcompeted by their wild-type counterpart. Moreover, monocyte-autonomous TNF is critical for the function of these cells, as *TNF* ablation in monocytes/macrophages, but not in microglia, delayed the onset of EAE in challenged animals and was associated with reduced acute spinal cord infiltration of Ly6C^{hi} effector monocytes. Collectively, our data reveal a previously unappreciated critical cell-autonomous role of *TNF* on monocytes for their survival, maintenance, and function.

INTRODUCTION

Monocytes are circulating mononuclear phagocytes and comprise two main subsets, which in mice have been defined as CCR2^{+} CX$_3$CR1^{int} CD43^{lo} Ly6C^{hi} and CCR2^{-} CX$_3$CR1^{hi} CD43^{hi} Ly6C^{lo} cells (Geissmann et al., 2003; Ginhoux and Jung, 2014; Mildner et al., 2016). Monocytes develop in steady state in the BM from common monocyte precursors (cMOPs; Hettinger et al., 2013) that themselves derive from monocyte/macrophage DC precursors (MDP; Fogg et al., 2006; Varol et al., 2007). Ly6C^{hi} monocytes are short lived (Yona et al., 2013) and poised to home to sites of inflammation to give rise to cells with DC or macrophage features (Mildner et al., 2013). Ly6C^{lo} cells are progeny of Ly6C^{hi} monocytes, display more extended half-lives (Yona et al., 2013), and are patrolling cells specialized in surveillance of vascular integrity (Auffray et al., 2007). As such, Ly6C^{lo} cells can be considered a blood-resident macrophage population (Ginhoux and Jung, 2014). Infiltrates of Ly6C^{hi} monocytes are prominent in neuroinflammatory disorders, such as the animal model of multiple sclerosis (MS), experimental autoimmune encephalomyelitis (EAE), which involves blood–brain barrier breakage (Mildner et al., 2009). Emerging evidence indicates distinct functional contributions of monocyte-derived cells and central nervous system (CNS)–resident microglia (Shechter et al., 2009; Ajami et al., 2011; Yamasaki et al., 2014).

Proinflammatory cytokines, such as *IL-1β*, *IL-6*, and *TNF*, are hallmarks of CNS inflammation (Murphy et al., 2010). *TNF* has pleiotropic actions and can induce both cell death and apoptosis resistance (Karin and Lin, 2002). In MS lesions, *TNF* is highly abundant and produced by many cells (Hofman et al., 1989; Bitsch et al., 2000). *TNF* is synthesized as a membrane-bound molecule but can be shed by the metalloprotease TNF-α–converting enzyme (*TACE*; Horiuchi et al., 2007). Both transmembrane and shed *TNF* isoforms have activity with partially distinct impact. Membrane-tethered *TNF* displays higher affinity for *TNFR2* (p75) and was proposed to predominantly promote cell survival (Grell et al., 1995), whereas shed TNF binds preferentially to the death domain containing *TNFR1* (p55), which may trigger apoptosis as shown in in vitro assays (Grell et al., 1998). Thus, TNF can act in diverse and even adverse ways (Caminero et al., 2011).

Using mice harboring conditional mutant *TNF* alleles, it was shown that TNF produced by myeloid cells mediates LPS-induced septic shock and protection from intracellular

Correspondence to Steffen Jung: s.jung@weizmann.ac.il

Abbreviations used: cMOP, common monocyte precursor; CNS, central nervous system; DSS, dextran sulfate sodium; EAE, experimental autoimmune encephalomyelitis; MACS, magnetic-activated cell sorting; MDP, monocyte/macrophage DC precursor; MS, multiple sclerosis; PI, propidium iodide; TAM, tamoxifen.

© 2017 Wolf et al. This article is distributed under the terms of an Attribution–Noncommercial–Share Alike–No Mirror Sites license for the first six months after the publication date (see http://www.rupress.org/terms/). After six months it is available under a Creative Commons License (Attribution–Noncommercial–Share Alike 4.0 International license, as described at https://creativecommons.org/licenses/by-nc-sa/4.0/).

The Rockefeller University Press $30.00
J. Exp. Med. 2017 Vol. 214 No. 4 905–917
https://doi.org/10.1084/jem.20160499

Supplemental material can be found at:
http://doi.org/10.1084/jem.20160499

The Journal of Experimental Medicine

Downloaded from jem.rupress.org on February 9, 2018

pathogens (Grivennikov et al., 2005). Moreover, when subjected to EAE, *lyzM*^{Cre}*:tnf*$^{fl/fl}$ mice displayed delayed disease initiation, though no amelioration of the subsequent chronic pathology (Kruglov et al., 2011). This suggested a specific role of myeloid *TNF* in EAE onset. However, as the LysM promoter displays activity in both neutrophils and monocytes and low penetrance in microglia (Goldmann et al., 2013), it remained unclear which myeloid cells produce the critical TNF and what the underlying mechanisms are.

Here, we investigate the importance of *TNF* signaling in steady-state and inflammatory monocytes. We reveal a novel critical role of autonomous *TNF* signaling as a survival factor for monocytes, both in steady state and under neuroinflammatory conditions. Moreover, using the $CX_3CR1^{Cre/CreER}$ system (Yona et al., 2013), we investigated the relative contribution of *TNF* derived from microglia or monocytes for EAE induction and show that microglial *TNF* is dispensable for EAE development. In contrast, absence of autonomous *TNF* from the monocyte infiltrate impaired survival of the cells and delayed EAE induction.

RESULTS AND DISCUSSION

Requirement of cell-intrinsic and -nonintrinsic TNF during monocyte development

Transcriptome analysis of monocytes and their BM precursors revealed a consistent, though modest, expression of *TNF*, which increases with the steady-state differentiation of Ly6C^{hi} monocytes into Ly6C^{lo} cells (Fig. 1, A and B; unpublished data). Moreover, with progression from the Ly6C^{hi} via the Ly6C^{int} to the Ly6C^{lo} stage, monocytes gradually increased expression of many NF-κB signature genes, including *tnf* and its receptors *tnfrsf1a* (encoding *TNFR1*) and *tnfrsf1b* (encoding *TNFR2*), as part of their conversion program (Fig. 1, A and B). *Tnfrsf1a* levels are high already at the MDP stage and increase moderately (about twofold) with monocyte development, whereas *tnfrsf1b* displays low expression in BM precursors but is ∼20-fold induced during development, peaking in Ly6C^{lo} blood monocytes. Interestingly, *TNF* expression levels are significantly correlated with expression of both *TNFR1* ($r = 0.597$; $P < 0.05$) and *TNFR2* ($r = 0.809$; $P < 0.001$).

TNFR1-deficient monocytes are present in similar numbers and subset distribution as monocytes in WT blood (Fig. S1 A). To probe for a potential role of *TNF* in monocyte generation and survival in a competitive setting, we generated mixed BM chimeras, in which lethally irradiated WT mice received equal amounts of WT BM (CD45.1) and BM deficient for either TNF receptor 1 (*TNFR1*$^{-/-}$) or both TNF receptors (*TNFR1/2*$^{-/-}$; CD45.2; Fig. 1, C and D; and Fig. S1 B). When analyzed after 4 wk, the blood T cell compartment of the chimeras displayed similar representation of both genotypes. However, *TNFR1*$^{-/-}$ Ly6C^{hi} monocytes (CD45.1/2 ratio ∼15-fold) and, even more profoundly, *TNFR1*$^{-/-}$ Ly6C^{lo} monocytes (CD45.1/2 ratio ∼50-fold) were outcompeted by their WT counterparts (Fig. 1 C). A similar effect was evident in [WT/*TNFR1/2*$^{-/-}$ > WT] BM chimeras, with an additive impact of the *TNFR2* mutation, which was significant in Ly6C^{lo} monocytes (CD45.1/2 ratio ∼75-fold), in line with their up-regulation of *TNFR2* (Fig. 1, C and D). Of note, examination of monocytic BM precursors, including MDP, cMOP, and BM Ly6C^{+} monocytes, also revealed an overrepresentation of the WT genotype (Fig. 1 D, and Fig. S1, C and D). This indicates TNF requirement during monopoiesis. However, the further bias among the Ly6C^{lo} blood monocytes of the [WT/*TNFR1/2*$^{-/-}$] chimeras, together with the up-regulation of both *TNF* and *TNFR2* in these cells, suggests an additional role of *TNF* in Ly6C^{hi} to Ly6C^{lo} monocyte conversion (Fig. 1 D).

These data raised the possibility that *TNF* has an autonomous effect on monocytes. To probe more rigorously such a scenario, we next generated mixed BM chimeras with *TNF*$^{-/-}$ (CD45.2) and *TNF*$^{+/+}$ (CD45.1) BM. Representations of *TNF*-sufficient and -deficient Ly6C^{hi} blood monocytes, as well as MDP, cMOP, and Ly6C^{hi} BM monocytes, in these chimeras were equal, indicating no requirement of autonomous *TNF* throughout monocyte development up to this point (Fig. 1, E and F; and Fig. S1 E). In contrast, *TNF*-deficient Ly6C^{lo} monocytes were significantly underrepresented as compared with *TNF*-sufficient monocytes (Fig. 1 F). Because these cells retain *TNF* receptor expression, these data imply an intrinsic requirement for cell-autonomous *TNF* by these monocytes.

Absence of TNF signaling leads to excessive monocyte cell death

Cell-autonomous *TNF* could be required for either monocyte development or survival. To test the latter option, we resorted to an in vitro microfluidic system (Zaretsky et al., 2012). Specifically, we isolated circulating Ly6C^{hi} and Ly6C^{lo} monocytes from WT, *TNF*$^{-/-}$, and *TNFR1*$^{-/-}$ mice and co-cultured them in microwells (Zaretsky et al., 2012) in the presence of the dead cell marker propidium iodide (PI) for 48 h (Fig. 2 A). Co-culture of WT and knockout monocytes in separate microwells in the same array allows for direct comparison of their death rate and survival, with single-cell resolution. In this assay, cells can initially respond only to *TNF* they secrete themselves; at later time points though, *TNF* can diffuse from *TNF*-secreting cells and affect cells in neighboring microwells with a typical diffusion time between wells of ∼24 h. The single-cell real-time analysis for cell death revealed that monocytes deprived of *TNFR1* died significantly more rapidly than their WT counterpart, including both Ly6C^{hi} and Ly6C^{lo} cells. Moreover, the fraction of cells surviving 48 h in culture was significantly lower compared with *TNFR1*-sufficient monocytes (Fig. 2, B–E). A similar result was obtained with *TNF*-deficient Ly6C^{hi} monocytes, which also exhibited faster death rates. However, the fraction of surviving cells at the end of the assay was similar to that of WT monocytes, probably because of TNF secreted by WT monocytes diffusing from neighboring microwells (Fig. 2, C–E). Earlier studies demonstrated that low doses of *TNF*

Downloaded from jem.rupress.org on February 9, 2018

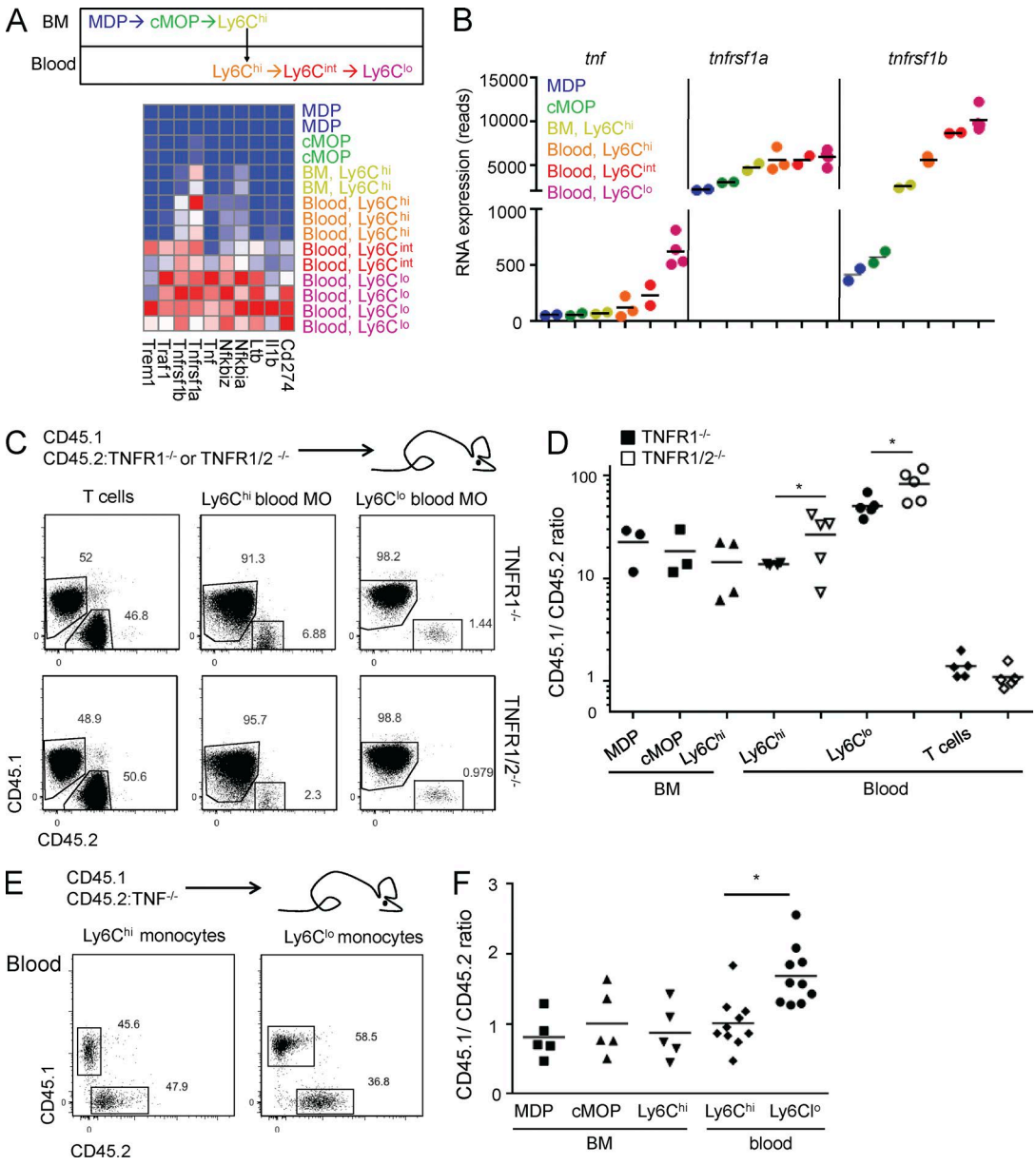

Figure 1. **Absence of TNF signaling impairs steady-state monocytes.** (A) Scheme illustrating monocyte development (top) and heat map of RNA sequencing expression data of NF-κB–driven genes in sorted MDP, cMOP, and Ly6C^{hi} BM monocytes, as well as Ly6C^{hi}, Ly6C^{int}, and Ly6C^{lo} blood monocytes (bottom). (B) RNA sequencing reads for *tnf*, *tnfrsf1a*, and *tnfrsf1b* expression throughout sequential monocyte development stages in A. n = 2–3. (C) FACS analysis of T cells and Ly6C^{hi} and Ly6C^{lo} monocytes (MO) extracted from blood of either [TNFR1$^{-/-}$/WT > WT] (top) or [TNFR1/2$^{-/-}$/WT > WT] (bottom) mixed BM chimeras. (D) Quantification of myeloid cells and precursors. n = 3–5. Mann-Whitney U test was used. (E) FACS analysis of Ly6C^{hi} and Ly6C^{lo} monocytes extracted from blood of [TNF/WT > WT] mixed BM chimeras. (F) Quantification of myeloid cells and precursors in C and D. n = 5–10. Student's t test was used. *, $P < 0.05$.

can promote myeloid cell survival (Cowburn et al., 2004; Lehner et al., 2012). After administration of 2.5 ng/ml exogenous recombinant TNF, both *TNF*-sufficient and -deficient Ly6C^{hi} monocytes were indeed partially rescued, as evident by a twofold increase of t_{half}, the time point at which the fraction of dying cells reached half of its maximal value, in both genotypes (Fig. 2 F; see Materials and methods for a description of t_{half} calculation). This effect was less substantial with a higher *TNF* dose (50 ng/ml; Fig. 2 F). Mixed cultures of MACS (magnetic-activated cell sorting)-sorted CD11b^{+}CD115^{+} BM monocytes from *TNFR*$^{-/-}$ (CD45.2) and *TNF*$^{-/-}$ (CD45.1) mice, treated with the macrophage differentiation factor M-CSF, showed no disadvantage of the *TNFR1*-deficient cells, indicating that autonomous *TNF* is

Downloaded from jem.rupress.org on February 9, 2018

dispensable for monocyte-derived macrophage differentiation (Fig. 2 G). In addition, cMOPs isolated from *TNF*$^{-/-}$ (CD45.2) and *TNF*$^{+/+}$ (CD45.1) mice displayed similar death rates and fractions of surviving cells, indicating that autonomous TNF is not required for monopoiesis (Fig. 2, H and I), corresponding to lack of *TNF* expression in cMOPs (Fig. 1, A and B). To relate these findings to the in vivo setting, we performed a staining for surface phosphatidylserine, as an indicator of cell death induction, on blood monocytes of the mixed chimeras. Interestingly, mutant Ly6C^{lo} monocytes in [WT/*TNF*$^{-/-}$ > WT] and [WT/*TNFR1*$^{-/-}$ > WT], i.e., cells deficient for either the cytokine or its receptor, displayed increased annexin V staining for the apoptotic marker as compared with WT cells, indicating that autonomous *TNF* is required for monocyte survival in vivo (Fig. 2, J and K).

In conclusion, the data obtained from the competitive in vivo experiments and the single-cell in vitro analysis established the requirement of autonomous *TNF* production of monocytes for their survival.

Ly6C^{hi} effector monocytes up-regulate TNF and TNFR1 during EAE

Monocyte infiltrates have been shown to play a critical role in the establishment of EAE that is distinct from microglia (Mildner et al., 2009; Ajami et al., 2011; Yamasaki et al., 2014). To investigate potential roles of monocyte- or macrophage-derived *TNF* in EAE development and probe for the physiological importance of the autonomous loop, we isolated the monocytic spinal cord infiltrate defined as CD45^{hi} CD11b^{+} Ly6C^{hi} Ly6G^{-} cells, hereafter termed effector monocytes (Mildner et al., 2013), from EAE-induced mice at the pre–EAE onset stage (day 9 after immunization; score 0; Fig. 3 A). The time point before onset of EAE paralysis was chosen to minimize secondary effects induced by demyelination and cell death. Comparative transcriptome analysis with Ly6C^{hi} steady-state monocytes (Lavin et al., 2014) revealed a list of 440 genes up-regulated in spinal cord effector monocytes compared with steady-state monocytes and 133 down-regulated genes, after filtering for genes displaying an absolute >1 log expression difference and p-value <0.01 (Fig. 3 B, and Tables S1 and S2). Canonical pathway analysis showed significant enrichment for inflammatory pathways, such as TLR, *IL-6*, and *TREM1* signaling, as well as Fcγ receptor-mediated phagocytosis and nitric oxide and reactive oxygen species production (Fig. 3 C). Among the genes up-regulated was *csfr2b*, encoding the GM-CSF receptor and recently shown to drive proinflammatory monocyte activity in EAE (Croxford et al., 2015), as well as *nr4a1*, which negatively regulates monocyte pathology in EAE (Shaked et al., 2015); moreover, we noted high expression of *tnfrsf1a* (*TNFR1*) and the nuclear protein *mki67*, indicating proliferation, as previously reported (Fig. 3, B and C; Ajami et al., 2011). Although only modestly expressed, *TNF* also was significantly induced in effector monocytes, as compared with robust myeloid genes such as *emr1* (encoding the F4/80 antigen), which was equally highly expressed in both populations (Fig. 3 D). Of note, *TNFR2* levels were moderately reduced in effector monocytes (Fig. 3 D).

Monocyte- but not microglia-derived TNF is critical for EAE onset

The up-regulation of *TNF* and *TNFR1* in effector monocytes mirrored the induction paralleling the generation of Ly6C^{lo} blood monocytes, suggesting a similar survival mechanism. To study the role of *TNF* expression for the function of mononuclear phagocytes in the context of EAE, we crossed *cx$_3$cr1*^{Cre} and *cx$_3$cr1*^{CreER} animals (Yona et al., 2013) to mice harboring floxed *tnf* alleles (Grivennikov et al., 2005). The *cx$_3$cr1*^{Cre} system broadly affects tissue macrophages, as well as monocyte-derived cells and a fraction of DCs (Yona et al., 2013; Aychek et al., 2015). However, the tamoxifen (TAM)-inducible *cx$_3$cr1*^{CreER} system targets long-lived cells that express the CX$_3$CR1 chemokine receptor at the time of TAM treatment. The latter includes microglia and nonparenchymal CNS macrophages (Goldmann et al., 2016) but excludes monocytes (Goldmann et al., 2013) and hence allows discrimination of microglial and monocyte-derived *TNF*. First, we investigated the EAE disease course in *cx$_3$cr1*^{Cre}*:tnf*$^{fl/fl}$ animals. To confirm the broad *TNF* deletion in tissue macrophages and monocytes, we challenged the animals with LPS, which is known to result in systemic *TNF* release (Grivennikov et al., 2005). *Cx$_3$cr1*^{Cre}*:tnf*$^{fl/fl}$ mice displayed 4 h after intraperitoneal LPS challenge significantly lower serum *TNF* levels than littermate controls (Fig. 3 E). To probe for EAE development in *cx$_3$cr1*^{Cre}*:tnf*$^{fl/fl}$ mice, we immunized the animals with MOG$_{35–55}$ peptide and monitored disease emergence up to day 70. Total myeloid-derived TNF was significantly reduced in *cx$_3$cr1*^{Cre}*:tnf*$^{fl/fl}$ mice in the spinal cord at EAE day 24 (Fig. 3 F), and *TNF* signal was abolished in both resident microglia and CD45^{hi}Ly6C^{hi} and CD45^{hi}Ly6C^{lo} monocytic infiltrates (Fig. S2 A). In accordance with earlier studies performed with *TNF*$^{-/-}$ animals (Kassiotis and Kollias, 2001; Kruglov et al., 2011), *cx$_3$cr1*^{Cre}*:tnf*$^{fl/fl}$ mice exhibited a delayed and less sharp EAE onset (mean day 31), as compared with *TNF*$^{fl/fl}$ controls, which showed an earlier and synchronized start (mean 14 d; Fig. 3, G and H). However, eventually, the severity of disease symptoms was comparable between the mutants and littermate controls, both with respect to the mean maximal score and extent of demyelination (Fig. 3 I and Fig. S2 E). Of note, when animals from several EAE experiments were pooled together, statistically significant effects were seen both with respect to disease onset and maximal severity, which was slightly reduced in *cx$_3$cr1*^{Cre}*:tnf*$^{fl/fl}$ animals (Fig. S2 B).

EAE development relies on generation of autoreactive CD4^{+} effector T cells, triggered by peripheral, and potentially also CNS-associated, DCs (Codarri et al., 2013). Delayed disease onset could indicate impaired T cell priming. However, analysis of lymph node T cells (day 6 after immunization) and spinal cord T cells of diseased animals (days 13 and 24) revealed

Downloaded from jem.rupress.org on February 9, 2018

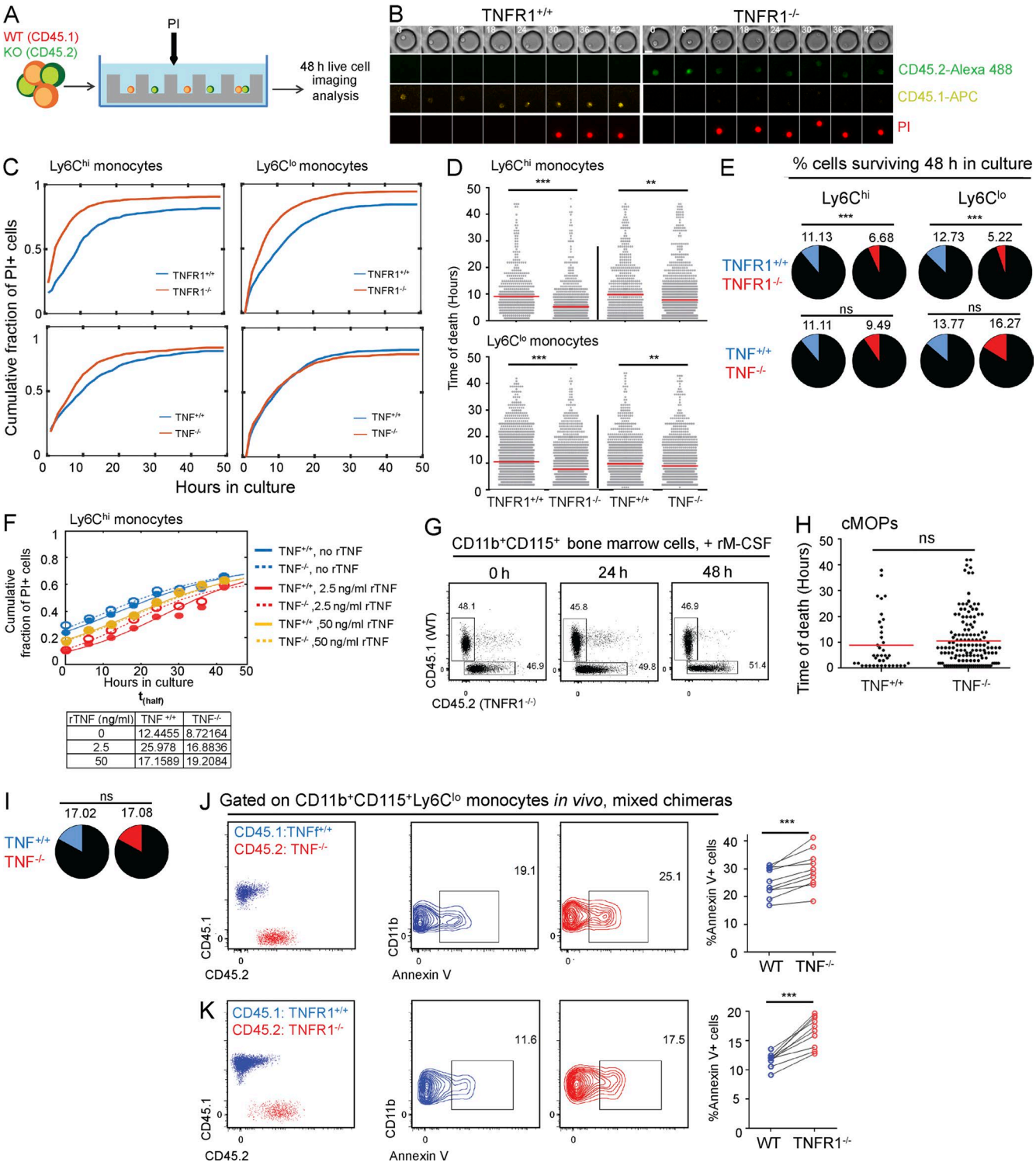

Figure 2. **Absence of TNF signaling increases apoptosis of circulating monocytes.** (A) Scheme of in vitro co-culturing of TNF/TNFR1-deficient and WT monocytes in microwells. (B) Traces of co-cultured WT (TNFR1$^{+/+}$) and TNFR1$^{-/-}$ monocytes monitored in culture for 48 h. WT/TNFR1$^{-/-}$ cells were distinguished by fluorescently labeled antibodies against CD45.1/CD45.2, respectively. Cell death time was monitored using PI. Bar, 10 µm. (C and D) Cumulative fraction of dead monocytes (PI^{+}) during 48 h (C) and timing of PI signal (indicating time of cell death) for individual cells (D) in co-cultures of: Ly6C^{hi} WT/TNFR1$^{-/-}$ monocytes (n = 567 and 960 cells, respectively), Ly6C^{hi} WT/TNF$^{-/-}$ (n = 641 and 1,348), Ly6C^{lo} WT/TNFR1$^{-/-}$ (n = 1,567 and 1,766), and Ly6C^{lo} WT/TNF$^{-/-}$ (n = 1,121 and 1,162). Red lines in D show means. **, $P < 0.01$; ***, $P < 0.001$. Mann-Whitney U test was used. (E) Fraction of monocytes surviving after 48 h of co-culture. ***, $P < 0.001$. χ^2 test was used. (F) Cumulative fraction of dead (PI^{+}) Ly6C^{hi} WT/TNF$^{-/-}$ monocytes co-cultured in microwell arrays

Downloaded from jem.rupress.org on February 9, 2018

similar numbers of $CD4^+$ effector T cells, as well as T helper 1 cell (Th1 cell) and Th17 cell prevalence in $cx_3cr1^{Cre}:tnf^{fl/fl}$ and $tnf^{fl/fl}$ mice. In addition, histology revealed no significant difference in $CD3^+$ cell numbers (Fig. S2, F and G). Finally, in vitro recall responses of lymph node $CD4^+$ effector T cells to secondary exposure to $MOG_{35–55}$ peptide, measured by the percentage of $CD44^+$ cells, were unaffected in $cx_3cr1^{Cre}:tnf^{fl/fl}$ mice (Fig. S2 H). Thus, the $CD4^+$ T cell compartment of $cx_3cr1^{Cre}:tnf^{fl/fl}$ mice is seemingly intact.

To investigate whether the EAE delay we observed in $cx_3cr1^{Cre}:tnf^{fl/fl}$ mice was caused by a lack of TNF production by monocyte-derived phagocytes or tissue-resident microglia, we resorted to the cx_3cr1^{CreER} system (Yona et al., 2013). First, we isolated microglia from TAM-treated $tnf^{fl/fl}$ and $cx_3cr1^{CreER}:tnf^{fl/fl}$ animals and challenged them ex vivo with 10 µg/ml LPS for 4 h. $Tnf^{fl/fl}$ microglia responded to stimulation with robust induction of *TNF*, whereas $cx_3cr1^{CreER}:tnf^{fl/fl}$ microglia failed to do so, confirming their lack of the *tnf* gene (Fig. S3 A). To investigate the impact of the microglial *TNF* deficiency on EAE development, $tnf^{fl/fl}$ and $cx_3cr1^{CreER}:tnf^{fl/fl}$ animals were immunized 6 wk after TAM treatment with $MOG_{35–55}$ peptide in CFA. Spinal cord microglia obtained from $MOG_{35–55}$-immunized $cx_3cr1^{CreER}:tnf^{fl/fl}$ mice lacked TNF production (Fig. S3, B and C). However, despite the prominent *TNF* expression in WT microglia, $cx_3cr1^{CreER}:tnf^{fl/fl}$ mice displayed an EAE disease course similar to that of littermate controls, both with respect to severity and onset (Fig. S3, D–F). No statistically significant change in day of onset or maximal severity was seen even when animals from several experiments were pooled together, despite a nonsignificant trend of reduced mortality in $cx_3cr1^{CreER}:tnf^{fl/fl}$ animals (Fig. S3, G and H). This establishes that microglial TNF is dispensable for EAE initiation in the $MOG_{35–55}$ peptide/CFA-induced C57BL/6 model.

Monocytic infiltrates are reduced in the absence of autonomous TNF

Neither peripheral T cell priming nor CNS infiltration of T cells seemed to depend on mononuclear phagocyte-derived *TNF*, and the microglia-restricted TNF deletion did not alter the disease course. Hence, we focused on the role of *TNF* production by CNS-infiltrating monocytes. In steady state, blood monocytes of $cx_3cr1^{Cre}:tnf^{fl/fl}$ mice display normal numbers (Fig. S2 C). A fraction of the WT ($tnf^{fl/fl}$) effector monocyte infiltrate in the spinal cords of diseased animals displayed *TNF* expression; however, as expected, the latter was absent from effector monocytes of $cx_3cr1^{Cre}:tnf^{fl/fl}$ mice (Fig. 4 A). Notably though, at day 9 after MOG immunization, i.e., before disease onset, and on day 24, effector monocyte numbers in spinal cords were found significantly reduced in $cx_3cr1^{Cre}:tnf^{fl/fl}$ mice, as compared with controls (Fig. 4, B and C). However, effector monocytes of $cx_3cr1^{Cre}:tnf^{fl/fl}$ mice expressed normal levels of MHC II, indicating similar activation of the cells in the absence of *TNF* (Fig. S2 D). Thus, we observed a positive correlation between numbers of $Ly6C^{hi}$ effector monocytes and their *TNF* expression and EAE onset.

The reduced number of infiltrating monocytes in the spinal cords of $cx_3cr1^{Cre}:tnf^{fl/fl}$ mice could stem from environmental impairment, such as reduced activation of endothelial cells, which are known to depend on *TNF* (Madge and Pober, 2001) and recruit monocytes via the CCL2/CCR2 axis (Paul et al., 2014). However, $CD31^+$ $CD45^-$ endothelial cells isolated from spinal cord of MOG-challenged $cx_3cr1^{Cre}:tnf^{fl/fl}$ mice and controls up-regulated expression of VCAM1, suggesting an unaltered endothelial response (Fig. S2 I). Alternatively, the reduction of effector monocytes in $cx_3cr1^{Cre}:tnf^{fl/fl}$ mice could result from autonomous *TNF*-mediated survival, similar to that observed for steady-state $Ly6C^{lo}$ monocytes. To probe this option, we generated mixed BM chimeras with $cx_3cr1^{Cre}:tnf^{fl/fl}$ (CD45.2) and $cx_3cr1^{gfp}:tnf^{+/+}$ (CD45.1) BM. [$Cx_3cr1^{Cre}:tnf^{fl/fl}/cx_3cr1^{gfp}:tnf^{+/+}$ > WT] mice were immunized with MOG peptide in CFA. Analysis of effector monocytes in the spinal cord 9 d after MOG immunization revealed an extensive out-competition of the *TNF*-deficient by the *TNF*-proficient (CD45.1) effector monocytes (Fig. 4 D). Interestingly, in dextran sulfate sodium (DSS)–induced colitis, an inflammatory condition in which monocytes do not up-regulate *TNF* (Zigmond et al., 2012), colonic $Ly6C^{hi}$ CD45.2 $tnf^{-/-}$ monocytes were represented in the same percentages as steady-state $Ly6C^{hi}$ blood monocytes, indicating that not all inflammatory conditions require autonomous *TNF* survival signal (Fig. S1 F). Collectively, these data show that absence of the autonomous *TNF* signal can have a critical impact on the performance of effector monocytes in both steady-state and inflammatory settings.

Here, we report the critical role of cell-intrinsic *TNF* for the survival and function of blood and effector monocytes in steady state and in a model of autoimmune neuroinflammation. The concept of cell-autonomous/

during 48 h without TNF (n = 80 and 164) or with 2.5 ng/ml (n = 192 and 142) or 50 ng/ml (n = 112 and 181) recombinant TNF (rTNF). Closed and open circles show data (WT and $TNF^{-/-}$, respectively), and continuous and dashed lines represent the best-fit logistic curve (see Materials and methods). The table shows t_{half}, the time by which the curves reach half of their maximum value. (G) FACS analysis of mixed cultures of MACS-sorted $CD115^+CD11b^+$ BM cells of CD45.1 and CD45.1/CD45.2 $TNFR1^{-/-}$ mice in the presence of 10 ng/ml M-CSF. Data are representative of three biological repeats. rM-CSF, recombinant M-CSF. (H and I) Timing of PI signal for individual cells (H) and fraction of cells surviving after 48 h (I) of cMOPs sorted from BM of WT and $TNF^{-/-}$ mice, co-cultured in microwell arrays. n = 47 and 170. (J and K) Fraction of annexin V^+ $Ly6C^{lo}$ monocytes in BM chimeric [TNF/WT > WT] (F) and [$TNFR1^{-/-}$/WT > WT] (G). n = 9–10. ***, P < 0.001. Paired Student's t test was used.

Downloaded from jem.rupress.org on February 9, 2018

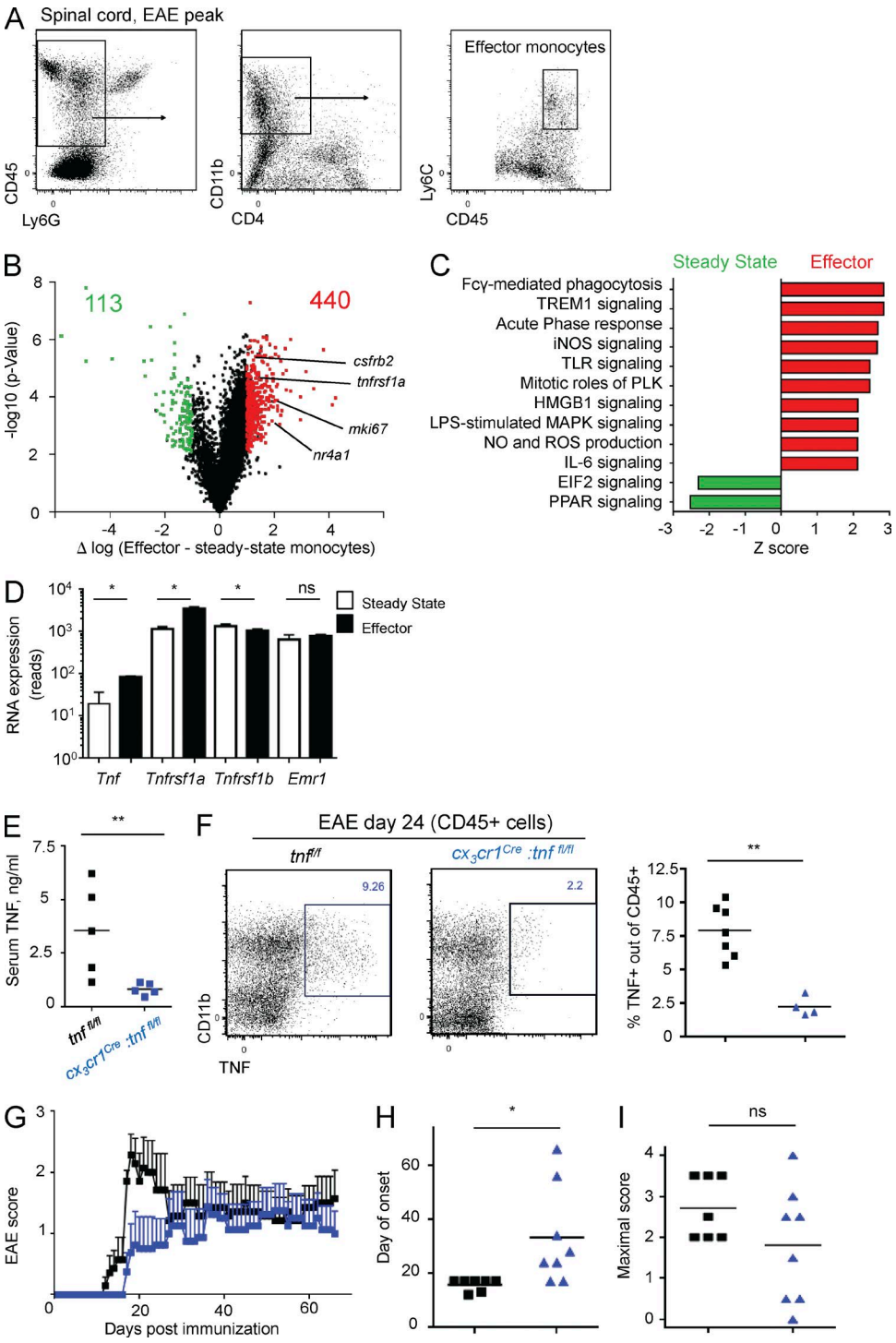

Figure 3. **Total monocyte/macrophage TNF deletion affects EAE onset.** (A) Gating strategy for spinal cord–infiltrating effector monocytes, used for all cell sorting and analysis. (B) Volcano plot performed for comparison of sorted steady-state blood monocytes and effector monocyte infiltrates in the spinal cord at EAE day 9. Numbers indicate genes significantly up-regulated (red) or down-regulated (green) in effector monocytes compared with steady-state monocytes (log difference >1 or <−1; $P < 0.05$). (C) Canonical pathway analysis performed for genes significantly changed in D. Z-score >2 or <−2. iNOS, inducible nitric oxide synthase; NO, nitric oxide; PLK, polo-like kinase; PPAR, peroxisome proliferator-activated receptor; ROS, reactive oxygen species. (D) Normalized reads of *tnf*, *tnfsr1a*, *tnfrsf1b*, and *emr1* expression in steady state and effector monocytes, as in Fig. 2 E. $n = 3$–4. Mann-Whitney *U* test was used. (E) ELISA of sera collected from *tnf*$^{fl/fl}$ and *cx*$_3$*cr1*^{Cre}:*tnf*$^{fl/fl}$ mice 4 h after intraperitoneal challenge with 200 µg LPS in vivo. $n = 5$. Mann-Whitney *U* test was used. (F) TNF production by myeloid cells in spinal cords of *tnf*$^{fl/fl}$ and *cx*$_3$*cr1*^{Cre}:*tnf*$^{fl/fl}$ mice at day 24 after $MOG_{35–55}$ immunization, analyzed by

Downloaded from jem.rupress.org on February 9, 2018

autocrine *TNF* signals has been discussed before in different cellular contexts. In cultured human monocyte-derived DCs, autocrine *TNF* was shown to inhibit apoptosis mediated by LPS and polyinosinic:polycytidylic acid, by regulating the balance between pro- and antiapoptotic proteins (Cowburn et al., 2004; Lehner et al., 2012). CpG-induced autocrine *TNF* of BM-derived mouse macrophages was suggested to amplify NF-κB activation (Caldwell et al., 2014). Moreover, LPS stimulation of these cells was recently shown to induce cell-intrinsic *TNF*-mediated necroptosis, if not inhibited by CYLD (Legarda et al., 2016). These experiments used primary cell cultures to dissect paracrine from autocrine *TNF* secretion. However, experimental evidence supporting the in vivo relevance and physiological implications of self-*TNF* and its impairment has been missing.

Specifically, here, we demonstrate that prosurvival signaling triggered by autonomous *TNF* is important for monocyte differentiation and monocyte maintenance. Of note, in the EAE model, inflammatory signals, which activate Ly6C^{hi} monocytes and recruit them to the site of inflammation, also initiate autocrine *TNF* as well as *TNFR1* expression. Moreover, *TNF* is found to be up-regulated after the conversion of Ly6C^{hi} monocytes into Ly6C^{lo} cells in the steady state, alongside the induction of its receptors, especially *TNFR2*. The *TNF*-triggered signal seems also important for the survival of effector Ly6C^{hi} monocytes infiltrating the spinal cord, as, in its absence, CNS monocyte numbers are reduced, and EAE disease development is delayed. Interestingly, BM monocyte precursors also require *TNF*, as indicated by the disadvantage of *TNFR1*-deficient cells compared with WT, but can acquire *TNF* from noncell-intrinsic origins and do not seem to express autonomous *TNF*.

Notably, we find TNF to be produced at levels that are detectable by flow cytometry only in a small fraction of effector monocytes; likewise, Ly6C^{lo} monocytes also express low amounts of *TNF*. However, interestingly, it has been reported that low concentrations of *TNF*, which could escape our readout, can promote survival, whereas high concentrations can confer apoptosis and collateral damage (van den Berg et al., 2001). This paradoxical effect of *TNF* on monocytes, i.e., promotion of survival or apoptosis at low and high levels, respectively, is reminiscent of an *IL-2* activity on T cells that we recently revealed as a mechanism that contributes to cell number homeostasis (Hart et al., 2014).

Although the deletion of myeloid *TNF* results in reduced monocyte numbers in the tissue, it does not significantly alter the extent of tissue damage caused by EAE; thus, monocyte-derived *TNF* is not required for demyelination itself. Likewise, microglial *TNF* is not required for the induction of EAE, probably because the massive generation of monocyte-derived macrophages can compensate for the loss of microglial *TNF*.

TNF is known primarily as a proinflammatory cytokine and a mediator of apoptosis (Wajant et al., 2003). However, *TNF* signaling activates the NF-κB signaling pathway, which also includes many genes promoting cell survival and inhibiting cell death by apoptosis (Karin and Lin, 2002). In human neutrophils, *TNF* can induce survival in an NF-κB–dependent manner (Cowburn et al., 2004). Moreover, human DCs were proposed to be protected by autocrine TNF from apoptosis, although in the performed in vitro assays, *TNF* provision by neighbor DCs could not be ruled out (Lehner et al., 2012).

Importantly, our study focuses on EAE disease onset. As our work is confined to C57BL/6 mice, we were bound to $MOG_{35–55}$ peptide vaccination and can draw no conclusions on a relapsing/remitting EAE course, which might arguably better reflect the disease progression in humans (Berard et al., 2010). Future work using SJL mice and other peptides, such as proteolipid protein and myelin basic protein, will be required to elucidate the roles of myeloid TNF in the remyelination process and of monocytic or microglial *TNF* in EAE reoccurrence.

An even more important question is whether the intrinsic TNF survival mechanism we report exists in human monocytes. *TNF* antagonist so far proved to be inefficient or even detrimental in EAE (Caminero et al., 2011). However, our data suggest that neutralization of monocytic *TNF*, either by a specific antagonist or by blockade of the corresponding receptor, could be tested clinically for its potential to ameliorate MS in humans. Of particular interest in this respect are newly developed bispecific antibodies designed to specifically neutralize monocyte/macrophage *TNF* (Efimov et al., 2016). *TNFR1*$^{-/-}$ mice are protected from EAE, and selective neutralization of *TNFR1* with antibody reduces disease severity (Williams et al., 2014). An alternative promising approach could be the monocyte-specific knockdown of *TNF* or its receptors by nanoparticle-encapsulated siRNA, as recently demonstrated for *CCR2* (Majmudar et al., 2013).

To conclude, here, we describe a novel role for cell-intrinsic *TNF* in the survival of monocytes under both steady-state and pathological conditions. We show that this autocrine signal can alter significantly the disease course in autoimmune demyelination and potentially other conditions that involve acute recruitment of effector monocytes.

MATERIALS AND METHODS

Mice

The following 4–24-wk-old mice were used: C57BL/6 (CD45.2 and CD45.1; B6.SJL-*Ptprca Pep3b*/Boyj; Jackson

FACS. $n = 7–4$. Mann-Whitney *U* test was used. (G–I) EAE disease course (G), day of onset (H), and individual maximal score (I) in *tnf*$^{fl/fl}$ and *cx*$_3$*cr1*^{Cre}:*tnf*$^{fl/fl}$ mice immunized with $MOG_{35–55}$ peptide. $n = 7–8$. Student's *t* test was used. Data are representative of three independent experiments. *, $P < 0.05$; **, $P < 0.01$. Results are expressed as means ± SEM.

Downloaded from jem.rupress.org on February 9, 2018

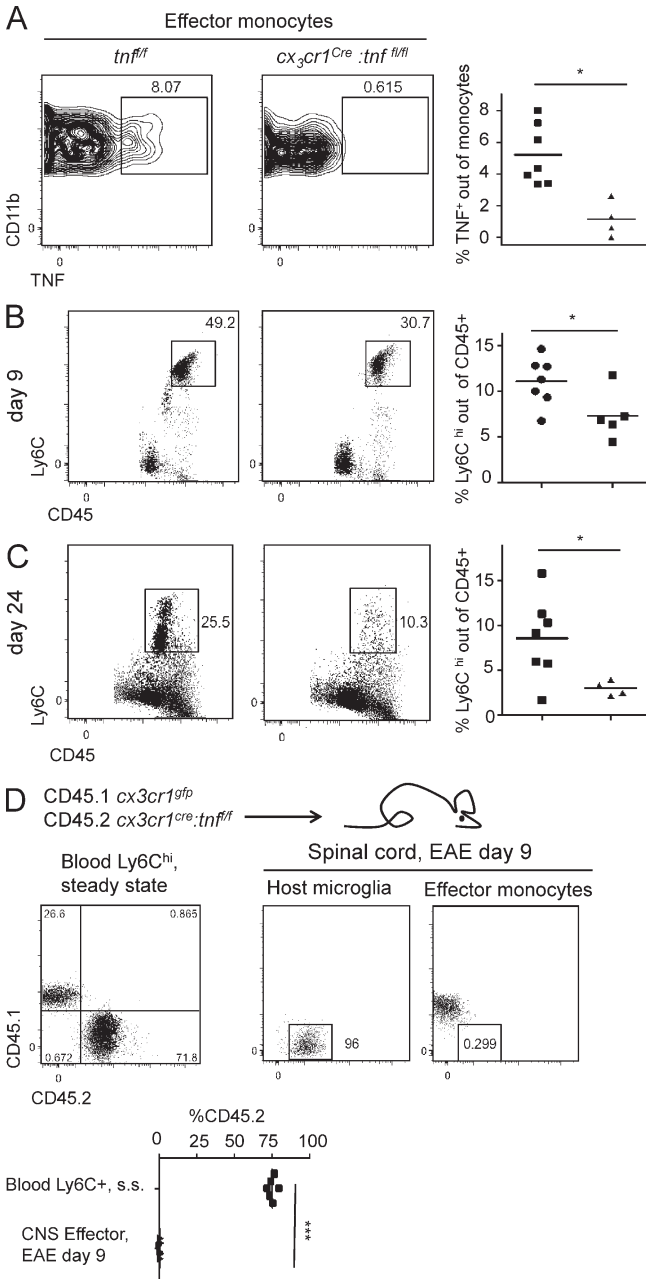

Figure 4. **Effector monocytes are reduced because of absence of autonomous TNF.** (A) FACS analysis of effector monocytes gated as in Fig. 3 A from MOG_{35-55} immunized in $tnf^{fl/fl}$ and cx_3cr1^{Cre}:$tnf^{fl/fl}$ mice at day 24. n = 4–7. Mann-Whitney U test was used. (B and C) FACS analysis of spinal cord $CD45^{hi}Ly6C^{hi}$ infiltrate in MOG_{35-55} immunized in $tnf^{fl/fl}$ and cx_3cr1^{Cre}:$tnf^{fl/fl}$ mice at day 9 (n = 5–7; B) or 24 (n = 4–7; C) after immunization. Mann-Whitney U test was used. (D) FACS analysis circulating steady-state (s.s.) $Ly6C^{hi}$ monocytes (gated as in Fig. S1 B) compared with spinal cord effector monocytes (gated as in Fig. 3 A) at day 9 after MOG_{35-55} immunization in [CD45.1 cx_3cr1^{gfp}:$tnf^{+/+}$/CD45.2 cx_3cr1^{Cre}:$tnf^{fl/fl}$ > CD45.2 WT] chimeric mice. Resident $CD45.2^+$ microglia (gated as in Fig. S3 B) are presented as reference cells for CD45.2 signal. n = 6. Student's t test was used. *, $P < 0.05$; ***, $P < 0.001$.

ImmunoResearch Laboratories, Inc.), $cx3cr1^{gfp/+}$ (JAX stock 005582 B6.129P-Cx3cr1tm1Litt/J; Jung et al., 2000), $cx3cr1^{Cre}$ (JAX stock 025524 B6J.B6N[Cg]-Cx3cr1tm1.1[cre] Jung/J), $cx3cr1^{CreER}$ (JAX stock 020940 B6.129P2[C]-Cx3cr1tm2.1[cre/ERT2]Jung/J; Yona et al., 2013), $tnf^{f/f}$ (Grivennikov et al., 2005), $tnf^{-/-}$ (Pasparakis et al., 1996), $tnfrsf1a^{-/-}$ ($TNFR1^{-/-}$; Rothe et al., 1993), and $tnfrsa1b^{-/-}$/$tnfrsf1b$ (TNFR1/2 DKO) mice (Probert et al., 2000). All animals were on a C57BL/6 background, maintained in specific pathogen–free conditions, and handled according to protocols approved by the Weizmann Institute Animal Care Committee as per international guidelines.

In vitro monocyte assays

Blood monocytes and BM cMOPs were sorted using a FAC SAria cell sorter (BD). Microwell arrays were designed using autoCAD (Autodesk Inc.) as an array of several hundreds of hexagonally spaced microwells, each being 25 µm in diameter and 60 µm in depth. Polydimethylsiloxane microwell arrays were fabricated using soft lithography as described previously (Zaretsky et al., 2012). The arrays were placed in glass-bottom 96-well plates. Monocytes were sorted and loaded into the microwell array: First, medium was removed and replaced with 25×10^3 monocytes in 100 µl RPMI medium. The plate was centrifuged at 300 g for 1 min to allow cells to settle in the microwells. Residual cells were aspirated, and wells were supplemented with 200 µl RPMI containing 0.5 ng anti-CD45.2–Alexa Fluor 488 and 0.5 ng anti-CD45.1–APC (BioLegend) and 2.5 µg/ml PI (Sigma-Aldrich) for a final dilution of $1:2 \times 10^5$ for the antibodies and $1:2 \times 10^3$ for PI (Zaretsky et al., 2012; Polonsky et al., 2016). For time-lapse experiments, a Ti-Eclipse microscope (Nikon) was used, equipped with an automated stage, incubator, and closed chamber that allows for CO_2 flow over the 96-well plate. Cells were imaged using a 20× objective and monitored using brightfield illumination and three fluorescence channels: FITC, Cy3, and Cy5. Time-lapse videos were collected using iQ software (Andor Technology). Image analysis was performed using a custom built MATLAB tool. Only microwells that included a single cell were included in the analysis. Analysis was performed in several steps: (a) identification of microwells using edge detection in the brightfield images, (b) background subtraction and illumination correction of fluorescent images, (c) identification of microwells, in which mean fluorescent intensities (MFIs) corresponded to that of a single cell (MFI values of single cells were evaluated manually for several hundreds of microwells in three different fields of view), and (d) death times were determined for each microwell as the time in which MFI in the Cy3 channel (PI signal) was ≥500. t_{half}, the time in which the cumulative death curve reaches half of its maximum value, was calculated by fitting the logistic equation

$$y = \frac{M}{1 + e^{-r \times (t - t_{half})}},$$

Downloaded from jem.rupress.org on February 9, 2018

in which M is the maximum value, and r is the steepness of the slope. Fitting was done using MATLAB. For the generation of monocyte-derived cells, BM of CD45.1 and CD45.2/ $tnf^{-/-}$ mice was extracted and flushed with PBS. The BM suspension was incubated with biotinylated CD115 antibody (BioLegend) and was MACS sorted using streptavidin beads (Miltenyi Biotec). The sorted cells were grown in RPMI medium containing 10% FCS, 1% L-glutamine, 1% penicillin/streptomycin, and 10 ng/ml M-CSF (PeproTech).

Generation of BM chimeras

7–10-wk-old recipient animals were lethally irradiated (950 rad) and reconstituted with donor BM by i.v. injection of a minimum of 10^6 BM cells. Donor BM was isolated from femurs and tibiae of donor mice, filtered through a 70-µm mesh, and resuspended in PBS for i.v. injection.

Reagent administration

TAM (Sigma-Aldrich) was dissolved in 10% ethanol/90% corn oil (Sigma-Aldrich) to a 100 mg/ml final solution. To induce Cre-mediated gene recombination in 5–7-wk-old *cx3cr1*^{creER}*:tnf*$^{f/f}$ mice, 5 mg TAM was administered orally for five consecutive days (25 mg total) by gavage. For EAE induction, mice were injected into each flank with 50 µl emulsion containing 1 mg/ml $MOG_{35–55}$ peptide (GeneScript), 1:4 PBS, and 1:2 Freund's incomplete adjuvant (Sigma-Aldrich) enriched with killed *Mycobacterium tuberculosis* (BD), supplemented with 250 ng pertussis toxin (Sigma-Aldrich) administered i.p. on days 0 and 2. For DSS-induced colitis, mice were administrated 2% DSS (MP Biomedicals) in drinking water for 7 d (Zigmond et al., 2012).

EAE assessment

EAE was assessed according to an accepted assessment index (Stromnes and Goverman, 2006). The mice were monitored daily by being held at the base of the tail. The index is as follows: 0, no symptoms; 0.5, partial tail limp; 1, complete tail limp; 1.5, impaired gait; 2, loss of pinch reflex in hindlimbs; 2.5, one hindlimb paralysis; 3, complete hindlimb paralysis; 3.5, one forelimb paralysis; 4, complete forelimb paralysis; and 5, death.

Tissue extraction and flow cytometry

For peripheral analysis, blood was collected by tail bleeds; mononuclear cells were enriched by Ficoll density gradient centrifugation at 1,000 *g* for 15 min at 20°C with low acceleration and no brake. For lymph node analysis, tissues were collected and digested for 1 h with 1 mg/ml collagenase D (Roche) in PBS containing magnesium and calcium ($PBS^{+/+}$; Beit Ha'emek) and then macerated mechanically and filtered through a 70-µm mesh. For CNS analysis, mice were perfused with 10 ml PBS via the left ventricle. Brain and spinal cord samples were harvested from individual mice, and tissues were homogenized and incubated with an HBSS solution containing 2% BSA (Sigma-Aldrich), 1 mg/ml collagenase D (Roche), and 0.15 mg/ml DNase1, filtered through a 70-µm mesh. Homogenized sections were resuspended in 40% percoll before density centrifugation (1,000 *g* for 15 min at 20°C with low acceleration and no brake). For spinal cord endothelium extraction, spinal cords were removed as for microglia extraction and digested with 0.1 mg/ml collagenase 11, 2 mg/ml collagenase 2, 0.2 mg/ml Dnase1, and 0.1 mg/ml hylurodinase 1 (Sigma-Aldrich). After cell suspension, cells were incubated in FACS buffer (PBS with 1% BSA, 2 mM EDTA, and 0.05% sodium azide) in the presence of staining antibody. For colon extraction after DSS, fecal content was flushed out with PBS, and the tissue was first incubated with HBSS containing 10% FCS, 2.5 mM EDTA, and 1 mM dithiothreitol. Next, the tissue was incubated with PBS containing 5% FCS, 1 mg/ml collagenase VIII (Sigma-Aldrich), and 0.1 mg/ml DNase I (Roche). For intracellular staining, the CytoFix/Cytoperm kit (BD) was used according to the instructions of the manufacturer. Cells were acquired on FACSCanto, LSRII, and LSRFortessa systems (BD) and analyzed with FlowJo software (Tree Star). For cell sorting, the FACSAria cell sorter (BD) was used. Antibodies used throughout the research are: CD11b (clone M1/70), CD45.1 (clone A20), CD45.2 (clone 104), B220 (clone RA3-6B2), CD115 (clone AFS98), Gr1 (clone RB6-8C5), Ly6C (clone AL21), Ly6G (clone H129.19), CD4 (clone H129.19), CD45 (clone 30F11), IL-17A (clone TC11-18H10.1), IFN-γ (clone XMG1.2), TNF (clone MP6-XT2), CD31 (clone 390), CD3 (clone 145-2C11), CD19 (clone 1D3/CD19), NK1.1 (clone PK136), VCAM1 (clone 429 MVCAM.A; all BioLegend), and F4/80 (clone BM8; Serotech).

RNA isolation, library construction, and analysis

RNA sequencing was performed as described previously (Jaitin et al., 2014). In brief, 10^3–10^4 cells from each population were sorted into 100–200 µl of lysis/binding buffer (Thermo Fisher Scientific). mRNA was captured with 12 µl of Dynabeads oligo(dT) (Thermo Fisher Scientific), washed, and eluted at 70°C with 10 µl of 10 mM Tris-Cl, pH 7.5. A mean of four million reads per library was sequenced and aligned to the mouse reference genome (NCBI 37; mm9) using TopHat (v2.0.10) with default parameters. Expression levels were calculated and normalized using ESAT software. RNA sequencing analysis focused on genes in the 25th percentile of expression with a twofold differential between at least two populations and a p-value <0.01. Canonical pathway analysis was performed using the Ingenuity program.

Ex vivo stimulation

For Th1/Th17 cell stimulation, spinal cord or lymph node samples were prepared as mentioned in the Tissue extraction and flow cytometry section and were incubated for 3 h in RPMI medium containing 10% FCS, 1:100 penicillin streptomycin antibiotic, 1:100 L-glutamine, 1:100 MEM, and 1:100 sodium pyruvate (Beit Ha'emek) supplemented with 20 µg/ml $MOG_{35–55}$ peptide (GeneScript). Then, the cell suspen-

Downloaded from jem.rupress.org on February 9, 2018

sions were further incubated with the same media, supplemented with 1 µg/ml brefeldin A (Sigma-Aldrich), for three additional hours before antibody staining. For ex vivo LPS stimulation, brain cell suspensions were incubated with the above RPMI medium supplemented with 10 µg/ml LPS for 2 h, followed by incubation in the presence of brefeldin A for an additional 2 h. Recombinant mouse TNF was purchased from PeproTech.

Histology

Histology was performed as described recently (Goldmann et al., 2013). In brief, mice were killed on day 24 after immunization and subsequently perfused with PBS. Subsequently, the spinal cords were removed, fixed in 4% buffered formalin, and embedded in paraffin. Then, tissue samples were sectioned and stained with Luxol fast blue (LFB-PAS) to assess the degree of demyelination and CD3 (1:100; MCA1477; AbD Serotec) to assess the degree of infiltration of T cells. Tissue sections were evaluated on a microscope (BX-61; Olympus) using cell-P software (Olympus).

ELISA

For ELISA, sera were extracted by tail bleed and centrifugation of blood at full speed for 7 min. TNF was measured using the DueSet kit (R&D Systems). ELISA was performed according to the manufacturer's instructions.

Statistical analysis

Results are expressed as means ± SEM. Statistical analysis was performed using Student's *t* test, Mann-Whitney *U* test, ANOVA, or repeated-measurements two-way ANOVA with posthoc Student's *t* test or paired Student's *t* test, as appropriate, using Prism (GraphPad Software).

Online supplemental material

Fig. S1 shows flow cytometric analysis of monocytes and monocyte precursors in the BM. Fig. S2 shows additional characterization of *cx3cr1*^{Cre}*:tnf*$^{f/f}$ mice. Fig. S3 shows microglia-restricted TNF deletion does not affect EAE onset. Tables S1 and S2 are included as Excel files. Table S1 lists genes up-regulated in spinal cord effector monocytes at EAE day 9 compared with Ly6C^{hi} monocytes. Table S2 lists genes down-regulated in spinal cord effector monocytes at EAE day 9 compared with Ly6C^{hi} monocytes.

ACKNOWLEDGMENTS

We would like to thank all members of the Jung laboratory for helpful discussion and the staff of the Weizmann Institute animal facility for excellent animal care.

Work in the Jung laboratory was supported by the Israel Science Foundation (grant 887/11), the Minerva Foundation (grant 711747), and the European Research Council (AdvERC grant 340345).

The authors declare no competing financial interests.

Submitted: 7 April 2016
Revised: 30 December 2016
Accepted: 15 February 2017

REFERENCES

Ajami, B., J.L. Bennett, C. Krieger, K.M. McNagny, and F.M.V. Rossi. 2011. Infiltrating monocytes trigger EAE progression, but do not contribute to the resident microglia pool. *Nat. Neurosci.* 14:1142–1149. http://dx.doi.org/10.1038/nn.2887

Auffray, C., D. Fogg, M. Garfa, G. Elain, O. Join-Lambert, S. Kayal, S. Sarnacki, A. Cumano, G. Lauvau, and F. Geissmann. 2007. Monitoring of blood vessels and tissues by a population of monocytes with patrolling behavior. *Science.* 317:666–670. http://dx.doi.org/10.1126/science.1142883

Aychek, T., A. Mildner, S. Yona, K.W. Kim, N. Lampl, S. Reich-Zeliger, L. Boon, N. Yogev, A. Waisman, D.J. Cua, and S. Jung. 2015. IL-23-mediated mononuclear phagocyte crosstalk protects mice from *Citrobacter rodentium*-induced colon immunopathology. *Nat. Commun.* 6:6525. http://dx.doi.org/10.1038/ncomms7525

Berard, J.L., K. Wolak, S. Fournier, and S. David. 2010. Characterization of relapsing-remitting and chronic forms of experimental autoimmune encephalomyelitis in C57BL/6 mice. *Glia.* 58:434–445. http://dx.doi.org/10.1002/glia.20935

Bitsch, A., T. Kuhlmann, C. Da Costa, S. Bunkowski, T. Polak, and W. Brück. 2000. Tumour necrosis factor alpha mRNA expression in early multiple sclerosis lesions: correlation with demyelinating activity and oligodendrocyte pathology. *Glia.* 29:366–375. http://dx.doi.org/10.1002/(SICI)1098-1136(20000215)29:4<366::AID-GLIA7>3.0.CO;2-Y

Caldwell, A.B., Z. Cheng, J.D. Vargas, H.A. Birnbaum, and A. Hoffmann. 2014. Network dynamics determine the autocrine and paracrine signaling functions of TNF. *Genes Dev.* 28:2120–2133. http://dx.doi.org/10.1101/gad.244749.114

Caminero, A., M. Comabella, and X. Montalban. 2011. Tumor necrosis factor alpha (TNF-α), anti-TNF-α and demyelination revisited: an ongoing story. *J. Neuroimmunol.* 234:1–6. http://dx.doi.org/10.1016/j.jneuroim.2011.03.004

Codarri, L., M. Greter, and B. Becher. 2013. Communication between pathogenic T cells and myeloid cells in neuroinflammatory disease. *Trends Immunol.* 34:114–119. http://dx.doi.org/10.1016/j.it.2012.09.007

Cowburn, A.S., J. Deighton, S.R. Walmsley, and E.R. Chilvers. 2004. The survival effect of TNF-α in human neutrophils is mediated via NF-κB-dependent IL-8 release. *Eur. J. Immunol.* 34:1733–1743. http://dx.doi.org/10.1002/eji.200425091

Croxford, A.L., M. Lanzinger, F.J. Hartmann, B. Schreiner, F. Mair, P. Pelczar, B.E. Clausen, S. Jung, M. Greter, and B. Becher. 2015. The Cytokine GM-CSF drives the inflammatory signature of CCR2^{+} monocytes and licenses autoimmunity. *Immunity.* 43:502–514. http://dx.doi.org/10.1016/j.immuni.2015.08.010

Efimov, G.A., A.A. Kruglov, Z.V. Khlopchatnikova, F.N. Rozov, V.V. Mokhonov, S. Rose-John, J. Scheller, S. Gordon, M. Stacey, M.S. Drutskaya, et al. 2016. Cell-type-restricted anti-cytokine therapy: TNF inhibition from one pathogenic source. *Proc. Natl. Acad. Sci. USA.* 113:3006–3011. http://dx.doi.org/10.1073/pnas.1520175113

Fogg, D.K., C. Sibon, C. Miled, S. Jung, P. Aucouturier, D.R. Littman, A. Cumano, and F. Geissmann. 2006. A clonogenic bone marrow progenitor specific for macrophages and dendritic cells. *Science.* 311:83–87. http://dx.doi.org/10.1126/science.1117729

Geissmann, F., S. Jung, and D.R. Littman. 2003. Blood monocytes consist of two principal subsets with distinct migratory properties. *Immunity.* 19:71–82. http://dx.doi.org/10.1016/S1074-7613(03)00174-2

Ginhoux, F., and S. Jung. 2014. Monocytes and macrophages: developmental pathways and tissue homeostasis. *Nat. Rev. Immunol.* 14:392–404. http://dx.doi.org/10.1038/nri3671

Goldmann, T., P. Wieghofer, P.F. Müller, Y. Wolf, D. Varol, S. Yona, S.M. Brendecke, K. Kierdorf, O. Staszewski, M. Datta, et al. 2013. A new type of microglia gene targeting shows TAK1 to be pivotal in CNS autoimmune inflammation. *Nat. Neurosci.* 16:1618–1626. http://dx.doi.org/10.1038/nn.3531

Downloaded from jem.rupress.org on February 9, 2018

Goldmann, T., P. Wieghofer, M.J. Jordão, F. Prutek, N. Hagemeyer, K. Frenzel, L. Amann, O. Staszewski, K. Kierdorf, M. Krueger, et al. 2016. Origin, fate and dynamics of macrophages at central nervous system interfaces. *Nat. Immunol.* 17:797–805. http://dx.doi.org/10.1038/ni.3423

Grell, M., E. Douni, H. Wajant, M. Löhden, M. Clauss, B. Maxeiner, S. Georgopoulos, W. Lesslauer, G. Kollias, K. Pfizenmaier, and P. Scheurich. 1995. The transmembrane form of tumor necrosis factor is the prime activating ligand of the 80 kDa tumor necrosis factor receptor. *Cell.* 83:793–802. http://dx.doi.org/10.1016/0092-8674(95)90192-2

Grell, M., H. Wajant, G. Zimmermann, and P. Scheurich. 1998. The type 1 receptor (CD120a) is the high-affinity receptor for soluble tumor necrosis factor. *Proc. Natl. Acad. Sci. USA.* 95:570–575. http://dx.doi.org/10.1073/pnas.95.2.570

Grivennikov, S.I., A.V. Tumanov, D.J. Liepinsh, A.A. Kruglov, B.I. Marakusha, A.N. Shakhov, T. Murakami, L.N. Drutskaya, I. Förster, B.E. Clausen, et al. 2005. Distinct and nonredundant in vivo functions of TNF produced by t cells and macrophages/neutrophils: protective and deleterious effects. *Immunity.* 22:93–104. http://dx.doi.org/10.1016/j.immuni.2004.11.016

Hart, Y., S. Reich-Zeliger, Y.E. Antebi, I. Zaretsky, A.E. Mayo, U. Alon, and N. Friedman. 2014. Paradoxical signaling by a secreted molecule leads to homeostasis of cell levels. *Cell.* 158:1022–1032. http://dx.doi.org/10.1016/j.cell.2014.07.033

Hettinger, J., D.M. Richards, J. Hansson, M.M. Barra, A.C. Joschko, J. Krijgsveld, and M. Feuerer. 2013. Origin of monocytes and macrophages in a committed progenitor. *Nat. Immunol.* 14:821–830. http://dx.doi.org/10.1038/ni.2638

Hofman, F.M., D.R. Hinton, K. Johnson, and J.E. Merrill. 1989. Tumor necrosis factor identified in multiple sclerosis brain. *J. Exp. Med.* 170:607–612. http://dx.doi.org/10.1084/jem.170.2.607

Horiuchi, K., T. Kimura, T. Miyamoto, H. Takaishi, Y. Okada, Y. Toyama, and C.P. Blobel. 2007. Cutting edge: TNF-α-converting enzyme (TACE/ADAM17) inactivation in mouse myeloid cells prevents lethality from endotoxin shock. *J. Immunol.* 179:2686–2689. http://dx.doi.org/10.4049/jimmunol.179.5.2686

Jaitin, D.A., E. Kenigsberg, H. Keren-Shaul, N. Elefant, F. Paul, I. Zaretsky, A. Mildner, N. Cohen, S. Jung, A. Tanay, and I. Amit. 2014. Massively parallel single-cell RNA-seq for marker-free decomposition of tissues into cell types. *Science.* 343:776–779. http://dx.doi.org/10.1126/science.1247651

Jung, S., J. Aliberti, P. Graemmel, M.J. Sunshine, G.W. Kreutzberg, A. Sher, and D.R. Littman. 2000. Analysis of fractalkine receptor CX3CR1 function by targeted deletion and green fluorescent protein reporter gene insertion. *Mol. Cell. Biol.* 20:4106–4114. http://dx.doi.org/10.1128/MCB.20.11.4106-4114.2000

Karin, M., and A. Lin. 2002. NF-κB at the crossroads of life and death. *Nat. Immunol.* 3:221–227. http://dx.doi.org/10.1038/ni0302-221

Kassiotis, G., and G. Kollias. 2001. Uncoupling the proinflammatory from the immunosuppressive properties of tumor necrosis factor (TNF) at the p55 TNF receptor level: implications for pathogenesis and therapy of autoimmune demyelination. *J. Exp. Med.* 193:427–434. http://dx.doi.org/10.1084/jem.193.4.427

Kruglov, A.A., V. Lampropoulou, S. Fillatreau, and S.A. Nedospasov. 2011. Pathogenic and protective functions of TNF in neuroinflammation are defined by its expression in T lymphocytes and myeloid cells. *J. Immunol.* 187:5660–5670. http://dx.doi.org/10.4049/jimmunol.1100663

Lavin, Y., D. Winter, R. Blecher-Gonen, E. David, H. Keren-Shaul, M. Merad, S. Jung, and I. Amit. 2014. Tissue-resident macrophage enhancer landscapes are shaped by the local microenvironment. *Cell.* 159:1312–1326. http://dx.doi.org/10.1016/j.cell.2014.11.018

Legarda, D., S.J. Justus, R.L. Ang, N. Rikhi, W. Li, T.M. Moran, J. Zhang, E. Mizoguchi, M. Zelic, M.A. Kelliher, et al. 2016. CYLD proteolysis protects macrophages from TNF-mediated auto-necroptosis induced by LPS and licensed by type I IFN. *Cell Reports.* 15:2449–2461. http://dx.doi.org/10.1016/j.celrep.2016.05.032

Lehner, M., B. Kellert, J. Proff, M.A. Schmid, P. Diessenbacher, A. Ensser, J. Dörrie, N. Schaft, M. Leverkus, E. Kämpgen, and W. Holter. 2012. Autocrine TNF is critical for the survival of human dendritic cells by regulating BAK, BCL-2, and FLIPL. *J. Immunol.* 188:4810–4818. http://dx.doi.org/10.4049/jimmunol.1101610

Madge, L.A., and J.S. Pober. 2001. TNF signaling in vascular endothelial cells. *Exp. Mol. Pathol.* 70:317–325. http://dx.doi.org/10.1006/exmp.2001.2368

Majmudar, M.D., E.J. Keliher, T. Heidt, F. Leuschner, J. Truelove, B.F. Sena, R. Gorbatov, Y. Iwamoto, P. Dutta, G. Wojtkiewicz, et al. 2013. Monocyte-directed RNAi targeting CCR2 improves infarct healing in atherosclerosis-prone mice. *Circulation.* 127:2038–2046. http://dx.doi.org/10.1161/CIRCULATIONAHA.112.000116

Mildner, A., M. Mack, H. Schmidt, W. Brück, M. Djukic, M.D. Zabel, A. Hille, J. Priller, and M. Prinz. 2009. $CCR2^{+}Ly\text{-}6C^{hi}$ monocytes are crucial for the effector phase of autoimmunity in the central nervous system. *Brain.* 132:2487–2500. http://dx.doi.org/10.1093/brain/awp144

Mildner, A., S. Yona, and S. Jung. 2013. A close encounter of the third kind: monocyte-derived cells. *Adv. Immunol.* 120:69–103. http://dx.doi.org/10.1016/B978-0-12-417028-5.00003-X

Mildner, A., G. Marinkovic, and S. Jung. 2016. Murine monocytes: Origins, subsets, fates, and functions. *Microbiol. Spectr.* 4.

Murphy, Á.C., S.J. Lalor, M.A. Lynch, and K.H.G. Mills. 2010. Infiltration of Th1 and Th17 cells and activation of microglia in the CNS during the course of experimental autoimmune encephalomyelitis. *Brain Behav. Immun.* 24:641–651. http://dx.doi.org/10.1016/j.bbi.2010.01.014

Pasparakis, M., L. Alexopoulou, V. Episkopou, and G. Kollias. 1996. Immune and inflammatory responses in TNF alpha-deficient mice: a critical requirement for TNF alpha in the formation of primary B cell follicles, follicular dendritic cell networks and germinal centers, and in the maturation of the humoral immune response. *J. Exp. Med.* 184:1397–1411. http://dx.doi.org/10.1084/jem.184.4.1397

Paul, D., S. Ge, Y. Lemire, E.R. Jellison, D.R. Serwanski, N.H. Ruddle, and J.S. Pachter. 2014. Cell-selective knockout and 3D confocal image analysis reveals separate roles for astrocyte-and endothelial-derived CCL2 in neuroinflammation. *J. Neuroinflammation.* 11:10. http://dx.doi.org/10.1186/1742-2094-11-10

Polonsky, M., B. Chain, and N. Friedman. 2016. Clonal expansion under the microscope: studying lymphocyte activation and differentiation using live-cell imaging. *Immunol. Cell Biol.* 94:242–249. http://dx.doi.org/10.1038/icb.2015.104

Probert, L., H.P. Eugster, K. Akassoglou, J. Bauer, K. Frei, H. Lassmann, and A. Fontana. 2000. TNFR1 signalling is critical for the development of demyelination and the limitation of T-cell responses during immune-mediated CNS disease. *Brain.* 123:2005–2019. http://dx.doi.org/10.1093/brain/123.10.2005

Rothe, J., W. Lesslauer, H. Lötscher, Y. Lang, P. Koebel, F. Köntgen, A. Althage, R. Zinkernagel, M. Steinmetz, and H. Bluethmann. 1993. Mice lacking the tumour necrosis factor receptor 1 are resistant to TNF-mediated toxicity but highly susceptible to infection by *Listeria* monocytogenes. *Nature.* 364:798–802. http://dx.doi.org/10.1038/364798a0

Shaked, I., R.N. Hanna, H. Shaked, G. Chodaczek, H.N. Nowyhed, G. Tweet, R. Tacke, A.B. Basat, Z. Mikulski, S. Togher, et al. 2015. Transcription factor Nr4a1 couples sympathetic and inflammatory cues in CNS-recruited macrophages to limit neuroinflammation. *Nat. Immunol.* 16:1228–1234. http://dx.doi.org/10.1038/ni.3321

Shechter, R., A. London, C. Varol, C. Raposo, M. Cusimano, G. Yovel, A. Rolls, M. Mack, S. Pluchino, G. Martino, et al. 2009. Infiltrating blood-derived macrophages are vital cells playing an anti-inflammatory role in recovery from spinal cord injury in mice. *PLoS Med.* 6:e1000113. http://dx.doi.org/10.1371/journal.pmed.1000113

Downloaded from jem.rupress.org on February 9, 2018

Stromnes, I.M., and J.M. Goverman. 2006. Passive induction of experimental allergic encephalomyelitis. *Nat. Protoc.* 1:1952–1960. http://dx.doi.org/10.1038/nprot.2006.284

van den Berg, J.M., S. Weyer, J.J. Weening, D. Roos, and T.W. Kuijpers. 2001. Divergent effects of tumor necrosis factor α on apoptosis of human neutrophils. *J. Leukoc. Biol.* 69:467–473.

Varol, C., L. Landsman, D.K. Fogg, L. Greenshtein, B. Gildor, R. Margalit, V. Kalchenko, F. Geissmann, and S. Jung. 2007. Monocytes give rise to mucosal, but not splenic, conventional dendritic cells. *J. Exp. Med.* 204:171–180. http://dx.doi.org/10.1084/jem.20061011

Wajant, H., K. Pfizenmaier, and P. Scheurich. 2003. Tumor necrosis factor signaling. *Cell Death Differ.* 10:45–65. http://dx.doi.org/10.1038/sj.cdd.4401189

Williams, S.K., O. Maier, R. Fischer, R. Fairless, S. Hochmeister, A. Stojic, L. Pick, D. Haar, S. Musiol, M.K. Storch, et al. 2014. Antibody-mediated inhibition of TNFR1 attenuates disease in a mouse model of multiple sclerosis. *PLoS One.* 9:e90117. http://dx.doi.org/10.1371/journal.pone.0090117

Yamasaki, R., H. Lu, O. Butovsky, N. Ohno, A.M. Rietsch, R. Cialic, P.M. Wu, C.E. Doykan, J. Lin, A.C. Cotleur, et al. 2014. Differential roles of microglia and monocytes in the inflamed central nervous system. *J. Exp. Med.* 211:1533–1549. http://dx.doi.org/10.1084/jem.20132477

Yona, S., K.W. Kim, Y. Wolf, A. Mildner, D. Varol, M. Breker, D. Strauss-Ayali, S. Viukov, M. Guilliams, A. Misharin, et al. 2013. Fate mapping reveals origins and dynamics of monocytes and tissue macrophages under homeostasis. *Immunity.* 38:79–91. http://dx.doi.org/10.1016/j.immuni.2012.12.001

Zaretsky, I., M. Polonsky, E. Shifrut, S. Reich-Zeliger, Y. Antebi, G. Aidelberg, N. Waysbort, and N. Friedman. 2012. Monitoring the dynamics of primary T cell activation and differentiation using long term live cell imaging in microwell arrays. *Lab Chip.* 12:5007–5015. http://dx.doi.org/10.1039/c2lc40808b

Zigmond, E., C. Varol, J. Farache, E. Elmaliah, A.T. Satpathy, G. Friedlander, M. Mack, N. Shpigel, I.G. Boneca, K.M. Murphy, et al. 2012. Ly6C hi monocytes in the inflamed colon give rise to proinflammatory effector cells and migratory antigen-presenting cells. *Immunity.* 37:1076–1090. http://dx.doi.org/10.1016/j.immuni.2012.08.026

Downloaded from jem.rupress.org on February 9, 2018

SUPPLEMENTAL MATERIAL

Wolf et al., https://doi.org/10.1084/jem.20160499

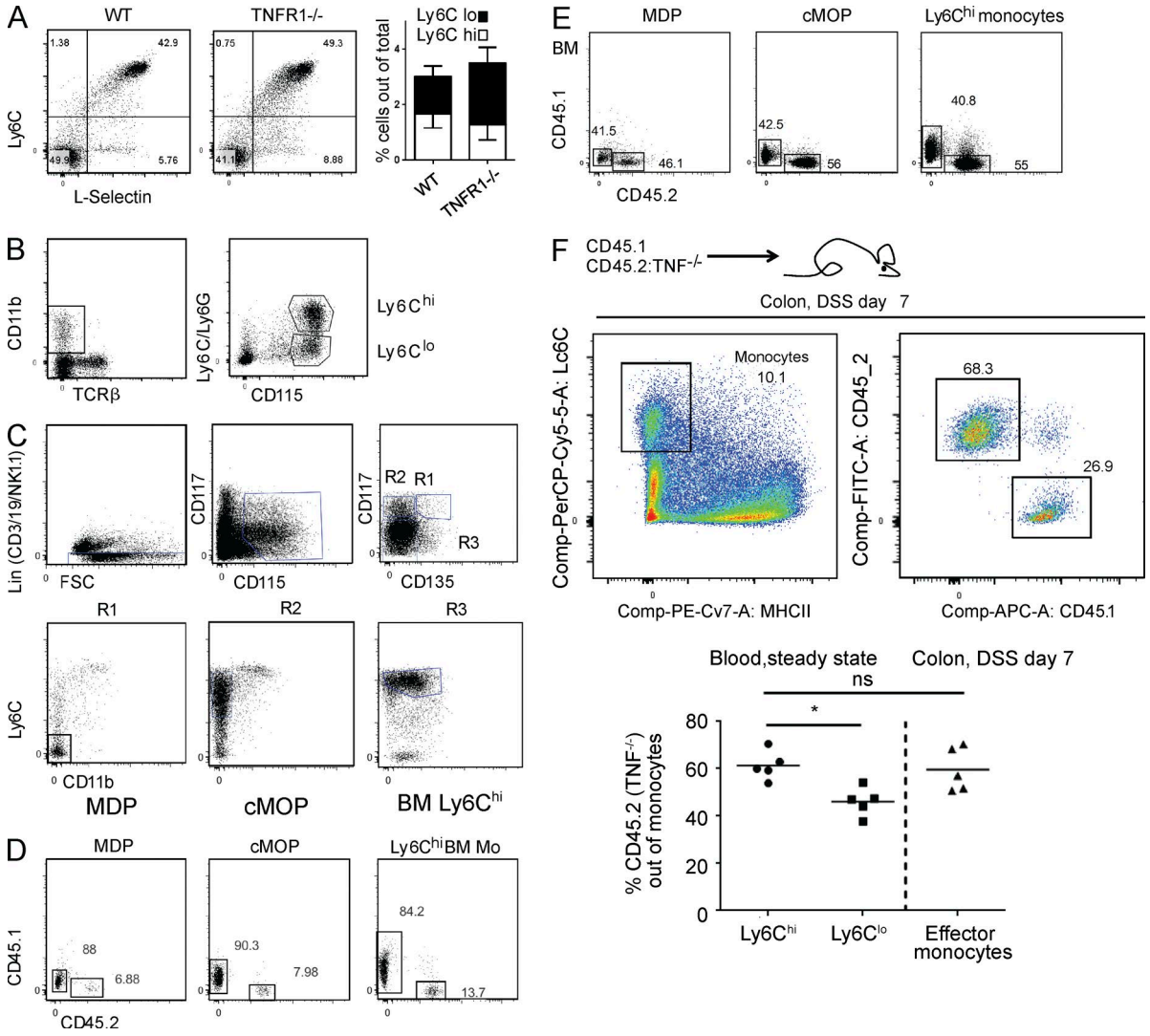

Figure S1. **Flow cytometric analysis of monocytes and monocyte precursors in the BM.** (A) FACS analysis of blood monocytes from nonchimeric WT and TNFR1$^{-/-}$ mice in steady state. $n = 8$. Results are expressed as means ± SEM. (B) FACS analysis illustrating definition of blood monocyte subsets. (C) FACS analysis illustrating definition of monocyte precursors. FSC, forward scatter. (D) FACS analysis of myeloid BM precursors: MDPs, cMOPs, and BM Ly6C^{hi} monocytes in [TNFR1$^{-/-}$/WT > WT] mixed BM chimeras. (E) FACS analysis of indicated myeloid BM precursors in [TNF/WT > WT] mixed BM chimeras as in F. Mo, monocyte. (F) FACS analysis of colons of [CD45.2 TNF$^{-/-}$/CD45.1 WT > WT] mice treated with 2% DSS for 7 d. Each mouse was assessed for frequency of CD45.2^{+} steady-state blood monocytes before DSS administration, as in Fig. 1 E. $n = 5$. *, $P < 0.05$; Mann-Whitney *U* test was used.

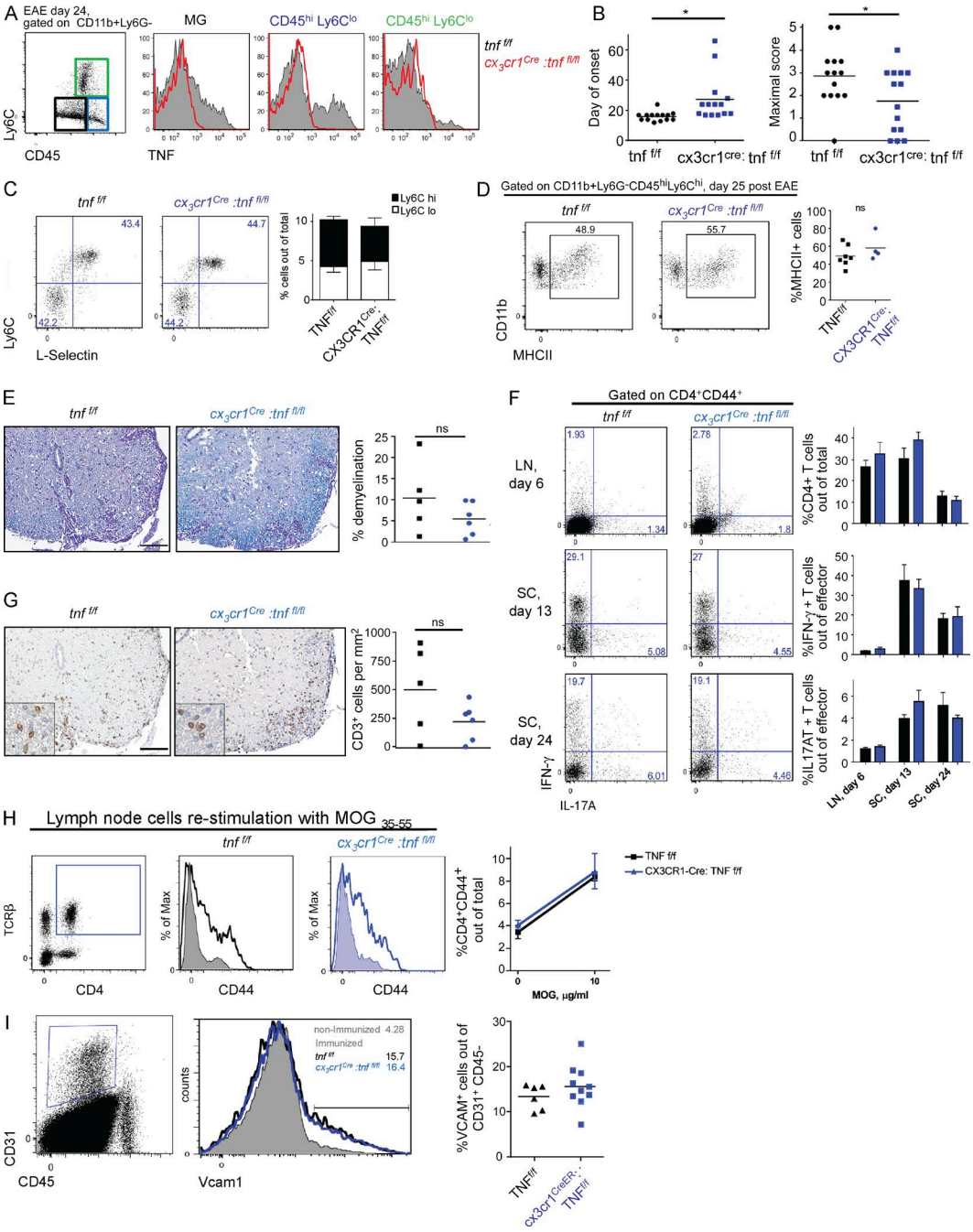

Figure S2. **Additional characterization of *cx3cr1*^{Cre}*:tnf*$^{f/f}$ mice.** (A) FACS analysis of intracellular TNF expression in different myeloid populations in the inflamed spinal cord of *tnf*$^{f/f}$ and *cx3cr1*^{cre}*:tnf*$^{f/f}$ mice. MG, microglia. (B) Pooled day-of-onset (left) and maximal-score (right) data of MOG_{35-55}-immunized *tnf*$^{f/f}$ and *cx3cr1*^{cre}*:tnf*$^{f/f}$ mice from three independent experiments. $n = 14$. *, $P < 0.05$. Student's *t* test was used. (C) FACS analysis of blood monocytes from *tnf*$^{f/f}$ and *cx3cr1*^{cre}*:tnf*$^{f/f}$ mice in steady state. $n = 8–7$. (D) FACS analysis of CD45^{hi}Ly6C^{hi}MHCII^{+} effector monocytes (gated as in Fig. 3 A) from spinal cords of MOG_{35-55}-immunized *tnf*$^{f/f}$ and *cx3cr1*^{cre}*:tnf*$^{f/f}$ mice 24 d after immunization (the same cells are shown also in Fig. 4 C). $n = 4–7$. (E) Histological analysis of demyelination by luxol-fast blue stain in spinal cords of in *tnf*$^{fl/fl}$ and *cx*$_3$*cr1*^{Cre}*:tnf*$^{fl/fl}$ mice at day 24 after immunization. $n = 5–6$. (F) FACS analysis of Th1 and Th17 cells in lymph nodes (LN) at day 6 after immunization or in spinal cord (SC) at days 13 and 24 in *tnf*$^{fl/fl}$ and *cx*$_3$*cr1*^{Cre}*:tnf*$^{fl/fl}$. $n = 4–6$. (G) CD3 histological stain in spinal cords of *tnf*$^{fl/fl}$ and *cx*$_3$*cr1*^{Cre}*:tnf*$^{fl/fl}$ mice at day 24 after immunization. $n = 5–6$. (E and G) Bars, 100 µm. (H) FACS analysis of lymph node T cells of *tnf*$^{fl/fl}$ and *cx*$_3$*cr1*^{Cre}*:tnf*$^{fl/fl}$ mice immunized with MOG_{35-55} in vivo and restimulated ex vivo with 10 µg/ml MOG_{35-55}. Shaded histograms represent nonstimulated cells. Unshaded histograms represent stimulated cells. $n = 3$ biological repeats. (I) FACS analysis for the activation marker VCAM1 on endothelial cells (CD31^{+}CD45) isolated from spinal cord of *tnf*$^{fl/fl}$ and *cx*$_3$*cr1*^{Cre}*:tnf*$^{fl/fl}$ mice 9 d after MOG_{35-55} immunization. $n = 6–10$. Results are expressed as means ± SEM.

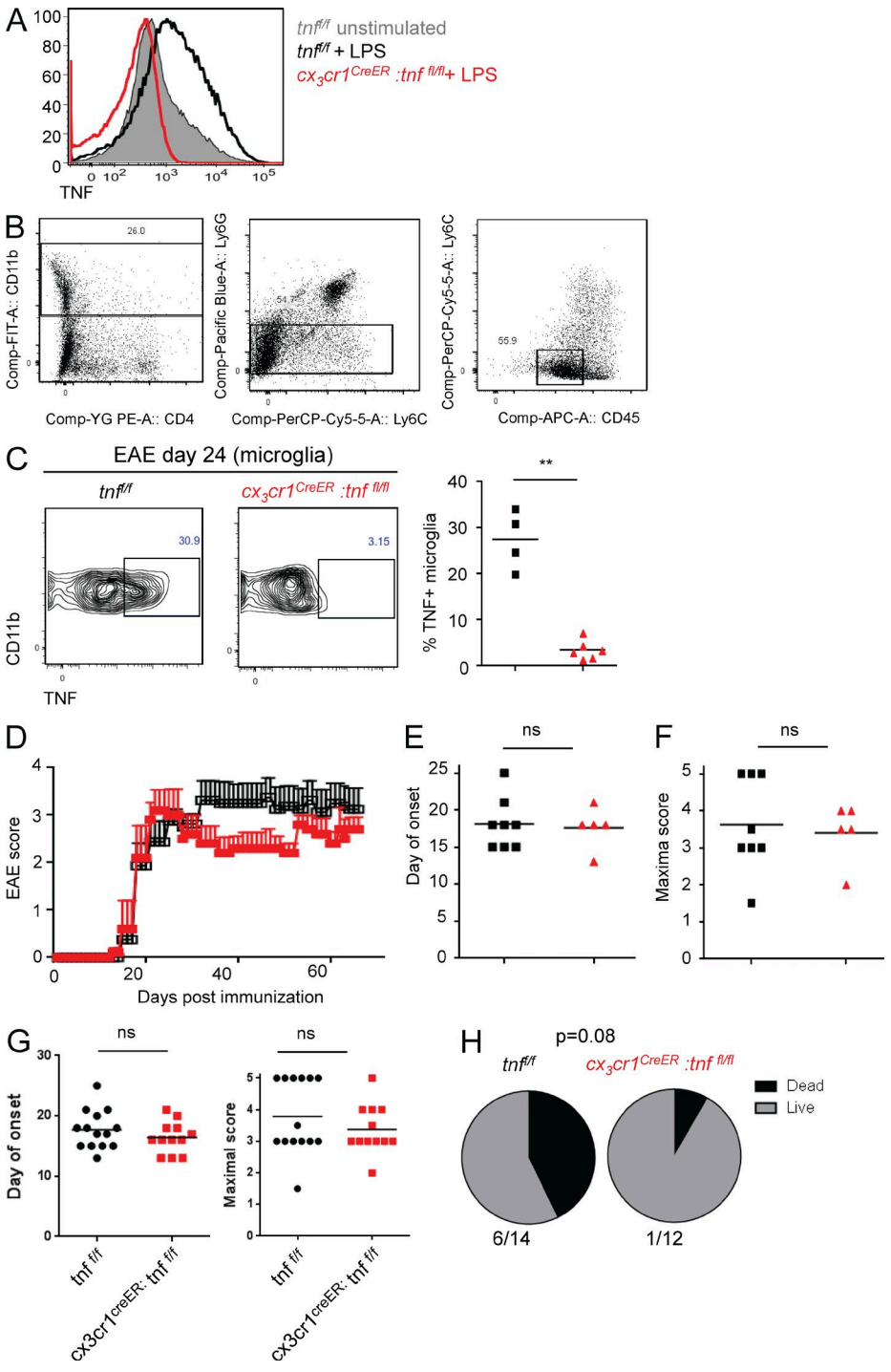

Figure S3. **Microglia-restricted TNF deletion does not affect EAE onset.** (A) Intracellular FACS staining for TNF expression of microglia isolated from *tnf*$^{fl/fl}$ and *cx*$_3$*cr1*^{CreER}*:tnf*$^{fl/fl}$ animals 6 wk after TAM treatment. Microglia were treated ex vivo with 10 µg/ml LPS for 4 h or left unstimulated. Data are representative of three biological repeats. (B) Gating strategy for microglia in the inflamed spinal cord. (C) TNF production by microglia (CD11b^{+}CD45^{int}Ly6C^{-}Ly6G^{-}) in spinal cords of TAM-treated *tnf*$^{fl/fl}$ and *cx*$_3$*cr1*^{CreER}*:tnf*$^{fl/fl}$ mice 24 d after MOG$_{35-55}$ immunization, analyzed by FACS. n = 4–6. **, P < 0.01. Mann-Whitney U test was used. (D–F) EAE disease course, individual day of onset, and individual maximal score of TAM-treated *tnf*$^{fl/fl}$ and *cx*$_3$*cr1*^{CreER}*:tnf*$^{fl/fl}$ mice immunized with MOG$_{35-55}$. n = 5–8. Data are representative of three independent experiments. Results are expressed as means ± SEM. (G) Pooled day of onset (left) and maximal score (right) of MOG$_{35-55}$-immunized *tnf*$^{f/f}$ and *cx3cr1*^{creER}*:tnf*$^{f/f}$ mice from three independent experiments. n = 12–14. (H) Mortality rate of pooled *tnf*$^{f/f}$ and *cx3cr1*^{creER}*:tnf*$^{f/f}$ mice shown in G. Numbers indicate the death incidence out of total mice in each group. χ test was performed to assess the significance.

Tables S1 and S2 are included as Excel files. Table S1 lists genes up-regulated in spinal cord effector monocytes at EAE day 9 compared with Ly6C^{hi} monocytes. Table S2 lists genes down-regulated in spinal cord effector monocytes at EAE day 9 compared with Ly6C^{hi} monocytes.